

Half-integer Mott-insulator phases in the imbalanced honeycomb lattice

Krzysztof Gawryluk,^{1,2} Christian Miniatura,^{3,1,4} and Benoît Grémaud^{5,1,4}

¹*Centre for Quantum Technologies, National University of Singapore, 3 Science Drive 2, Singapore 117543, Singapore*

²*Wydział Fizyki, Uniwersytet w Białymstoku, ul. Lipowa 41, 15-424 Białystok, Poland*

³*Institut Non Linéaire de Nice, UMR 7335, UNS, CNRS; 1361 route des Lucioles, 06560 Valbonne, France*

⁴*Department of Physics, National University of Singapore, 2 Science Drive 3, Singapore 117542, Singapore*

⁵*Laboratoire Kastler Brossel, Ecole Normale Supérieure CNRS, UPMC; 4 Place Jussieu, 75005 Paris, France*

(Dated: February 18, 2013)

Using mean-field theory, we investigate the ground state properties of ultracold bosons loaded in a honeycomb lattice with on-site repulsive interactions and imbalanced nearest-neighbor hopping amplitudes. Taking into account correlations between strongly coupled neighboring sites through an improved Gutzwiller ansatz, we predict the existence of half-integer Mott-insulator phases, i.e. states with half-integer filling and vanishing compressibility. These new insulating phases result from the interplay between quantum correlations and the topology of the honeycomb lattice, and could be easily addressed experimentally as they have clear signatures in momentum space.

Since its first experimental observation, graphene and its remarkable low-energy excitations have sparked a whole new branch of research comprising massless Dirac fermions, the anomalous quantum Hall effect and spin liquids to cite a few [1–3]. These discoveries have found a large echo in the field of ultracold atoms loaded in optical potentials [4, 5], be it for bosons [6, 7] or fermions [8, 9]. In this Letter, we address the bosonic Mott-Insulator to superfluid (MI-SF) transition in the honeycomb lattice. Though widely studied for the square lattice [10–15], we argue here that this transition is richer for graphene because of its peculiar topology [16]. Indeed, contrary to the square lattice, the honeycomb lattice is a genuine bipartite lattice made of two shifted triangular sub-lattices, one labeled with A sites and the other with B sites. The honeycomb Bravais unit cell thus possesses two sites and one can define symmetric and antisymmetric states in the unit cell. This has dramatic consequences for the ground state of the interacting system, in either the Mott or the superfluid phases. Strikingly, the repulsive Bose-Hubbard model on the honeycomb lattice features Mott phases at *half-integer* fillings when nearest-neighbor hopping amplitudes are imbalanced. In the following, we will present our model Hamiltonian and explain how to improve the usual mean-field approach [17–19] to correctly capture the crucial inter-sublattice correlations responsible for the half-integer Mott lobes. We will next compute the critical value of the MI-SF transition as a function of the imbalanced hopping parameter. Finally, we will show that these half-filled Mott phases have clear signatures in momentum space, making them easy to identify experimentally.

In the graphene lattice, each A site is connected to its three adjacent B sites by three vectors \mathbf{c}_α ($\alpha = 1, 2, 3$) summing up to zero [5]. Their common length define the lattice constant a that we set here to unity for convenience. We investigate the situation where the hopping parameter J' along \mathbf{c}_1 -links can be tuned and made dif-

ferent from the two other identical hopping parameters J along \mathbf{c}_2 and \mathbf{c}_3 -links. The limit $J' \ll J$ corresponds to weakly-coupled 1D-chains, whereas the limit $J' \gg J$ corresponds to weakly-coupled dimers. It is worth noticing that hopping imbalance in the graphene lattice has already been achieved experimentally [6–9]. Under these conditions, the tight-binding Bose-Hubbard Hamiltonian [20] with on-site repulsive interactions reads:

$$H = -J' \sum_{\ell} [a_{\ell}^{\dagger} b_{\ell} + b_{\ell}^{\dagger} a_{\ell}] - J \sum_{\langle \ell, \ell' \rangle} [a_{\ell}^{\dagger} b_{\ell'} + b_{\ell'}^{\dagger} a_{\ell}] + \frac{U}{2} \sum_{\ell} [\hat{n}_a^{\ell} (\hat{n}_a^{\ell} - 1) + \hat{n}_b^{\ell} (\hat{n}_b^{\ell} - 1)] - \mu \sum_{\ell} [\hat{n}_a^{\ell} + \hat{n}_b^{\ell}]. \quad (1)$$

Here a_{ℓ}^{\dagger} (a_{ℓ}) and b_{ℓ}^{\dagger} (b_{ℓ}) represent the creation (annihilation) operators associated with the A and B sites on a \mathbf{c}_1 -link hereafter labelled ℓ . The corresponding number operators are $\hat{n}_a^{\ell} = a_{\ell}^{\dagger} a_{\ell}$ and $\hat{n}_b^{\ell} = b_{\ell}^{\dagger} b_{\ell}$. The (positive) interaction strength is U and μ is the chemical potential. The summations run over all links ℓ and, in the kinetic term, over their nearest-neighbor \mathbf{c}_1 -links ℓ' such that the A-site on ℓ and the B-site on ℓ' are nearest neighbors [5]. For a given \mathbf{c}_1 -link, there are four such neighboring \mathbf{c}_1 -links.

In the following, we investigate the zero-temperature phase diagram of Eq.(1) within a mean-field approach [17, 18, 21]. We mainly restrict our analysis to the dimer regime $J' > J$. As long as $J' < 2J$, the band structure of the non-interacting case ($U = 0$) depicts the celebrated conical intersections at the Dirac points around $E = 0$ and the system is a semi-metal. At $J' = 2J$, the two Dirac points merge and the band structure undergoes a topological metal-insulator transition [5, 22]: when $J' > 2J$, the band structure consists of two bands separated by $2(J' - 2J)$. When $J \ll J'$, this is simply the energy difference obtained between the symmetric and antisymmetric dimer states $|\pm\rangle = (|A\rangle \pm |B\rangle)/\sqrt{2}$ (energy $\mp J'$) built on each \mathbf{c}_1 -link. These dimer states then

give rise to the two preceding bands, each with a width $4J$ independent of J' . In this weak interlink coupling regime (or strong dimer regime), we expect the physics to be driven by the lower band and the MI-SF phase transition to be controlled by the ratio J/U . In a mean-field approach, the Mott ground state is then well approximated by $\prod_{\ell} |n, \ell+\rangle$, where $|n, \ell+\rangle$ is the Fock state with n bosons in the symmetric state of link ℓ . This ground state cannot be written as a product of on-site states. As such, it is beyond reach of the standard Gutzwiller's ansatz. This salient feature directly arises from the 2-point topology of the graphene lattice and cannot happen with the square lattice where a strong imbalance of one hopping parameter leads to weakly-coupled 1D chains. A simple way to improve on the Gutzwiller's ansatz is to take into account correlations between neighboring lattice sites. This can be done in two ways by writing the (normalized) ground state as $|GS\rangle = \prod_{\ell} |\ell\rangle$:

$$|\ell\rangle = \sum_{n,m} f_{n,m}^{(\ell)} |n, A; m, B\rangle_{\ell} \quad (\text{with } \sum_{n,m} |f_{n,m}^{(\ell)}|^2 = 1) \quad (2)$$

$$= \sum_{p,q} g_{p,q}^{(\ell)} |p, +; q, -\rangle_{\ell} \quad (\text{with } \sum_{p,q} |g_{p,q}^{(\ell)}|^2 = 1), \quad (3)$$

where $|n, A; m, B\rangle_{\ell}$ is the Fock state on the link ℓ with n atoms occupying the A site and m atoms the B site while $|p, +; q, -\rangle_{\ell}$ is the Fock state on the same link ℓ with p atoms occupying the symmetric state $|+\rangle$ and q atoms the anti-symmetric state $|-\rangle$. If both preceding equations represent the most general two-site state, and therefore fully describes the system on each \mathbf{c}_1 -link, the parametrization Eq.(3) proves more useful in the limit $J' \gg J$. It is straightforward to compute the transformation between the two set of amplitudes $f_{n,m}^{(\ell)}$ and $g_{p,q}^{(\ell)}$ by noting that the annihilation and creation operators for the $|\pm\rangle$ states are simply $d_{\ell,\pm}^{(\dagger)} = (a_{\ell}^{(\dagger)} \pm b_{\ell}^{(\dagger)})/\sqrt{2}$.

The ground state of Eq.(1) has been obtained by imaginary-time evolution of an initial state with random values of amplitudes and periodic boundary conditions. As the structure of the corresponding nonlinear time-dependent equations [10, 23] is rather involved, a 4th-order Runge-Kutta method was necessary. We have carefully checked that our results were independent of the values of numerical parameters such as the number of sites, the time-step, the initial value of the amplitudes and the maximum occupancy number in the Fock states.

Uncoupled dimers. We consider first the situation $J = 0$ and solve for the on-link dimer problem. Figure 1 shows the on-site (left) and symmetric (right) average occupation numbers and their variances as a function of the chemical potential μ and hopping amplitude J' in units of the interaction strength U . For small J'/U values, the on-site density depicts the usual Mott plateaus at integer fillings. But, when J'/U increases, one clearly observes the appearance of new plateaus at half-integer fillings. At the same time, plateaus at odd integer values

$2p+1$ start to appear in the symmetric state density. For larger J'/U values, each of these plateaus splits in two new ones with $2p+1$ and $2p+2$ fillings. Correspondingly (but not shown here), the occupation number of the anti-symmetric state decreases from the same value $2p+1$ at $J' = 0$, to an almost vanishing value. The evolution of the on-site and symmetric variances emphasizes that the ground state of the system evolves from a on-site Fock state to an (almost) Fock state in the $|\pm\rangle$ basis when J'/U is cranked up. Indeed, for $J' \approx 0$, the on-site variance is almost zero, whereas the variance in the symmetric state is the largest. When J'/U is increased, the on-site variance gets larger, whereas the symmetric one almost vanishes. More precisely, for $J' \approx 0$, the ground state is well approximated by Fock states $|n, A; n, B\rangle_{\ell}$, whereas for larger value of J' , it is well approximated by Fock states $|p, +; 0, -\rangle_{\ell}$. One may however note that, for $J' = 0.6$, the symmetric variance, albeit extremely small, is not strictly zero and even increases with the chemical potential μ . This points at a slight contamination of the ground state at finite J' by the anti-symmetric states due to the interacting part of the Hamiltonian (1). Indeed, in the $|\pm\rangle$ basis, only the latter is not diagonal and a careful inspection shows that it couples states $|p, +; q, -\rangle_{\ell}$ with the same total number of atoms $p+q$, and only changes p and q by steps of two. As a consequence, the actual ground state rather reads:

$$|GS\rangle_{\ell} = \alpha |p, +; 0, -\rangle_{\ell} + \sum_{q \leq p/2} \alpha_q |p-2q, +; 2q, -\rangle_{\ell}. \quad (4)$$

In the large J'/U limit, α is of the order of unity, whereas the other coefficients are small and becoming smaller with either increasing q or J'/U . Except for $p = 0$ and $p = 1$, n_{\pm}^{ℓ} is always a bit less than an integer and the symmetric variance is never strictly zero, even if the discrepancies goes to 0 when increasing J'/U . This is clearly seen in plot (f) of Fig. 1 at $J' = 0.6$ (dot-dashed line) where the variance deviates from zero only for plateaus with symmetric filling $p \geq 2$ (solid line). For small J'/U values, the ground state simply becomes $|n, A; n, B\rangle_{\ell}$, such that the coefficients α_q are now given, up to a normalization factor, by $(-1)^q/(n-q)!q!$. They reach a maximum for $q = n/2$, leading to the same number of bosons in the $|\pm\rangle$ states. This corresponds to a ground state with an even-integer symmetric filling $p = 2n$ in Eq. (4). The case $p = 2n+1$ corresponds to an odd number of bosons and Eq. (4) is not a ground state of the system for $J' = 0$. However, for large enough J'/U , the additional energy cost for this extra boson is compensated for by the lowering of the symmetric state energy. It then becomes more favorable, in a given range of μ/U , to have the $2n+1$ bosons filling that state. Of course, the full transition when J'/U is increased is slightly more complicated since, at intermediate values, the ground state does not simply corresponds to a pure Fock state, either in the $|\pm\rangle$ basis or in the on-site one.

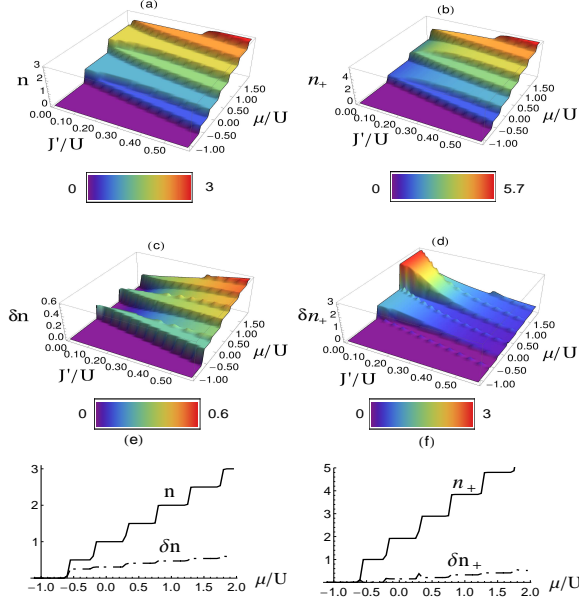


Figure 1. (color online). Phase diagram of Hubbard Hamiltonian (1) for $J = 0$. Left: plots of the on-site density n (a) and variance δn (c) as a function of J'/U and μ/U with their color codes. Plot (e) is a cut of (c) for $J'/U = 0.6$. Right: same as left but for the symmetric density n_+ and variance δn_+ . For large J'/U values, the on-site density depicts plateaus at half-integer fillings, corresponding to integer occupation numbers of the symmetric state $|+\rangle$. The bottom plots emphasize that the first plateau corresponds to the state $|1, +; 0, -\rangle_\ell$.

Coupled dimers. We now consider the $(J'/U, \mu/U)$ phase diagram in the symmetric state when the hopping amplitude J is non zero. As depicted by Fig. 2a and Fig. 2b, the situation is very much similar to the usual MI-SF transition. One finds regions with constant symmetric occupation numbers n_+ and almost vanishing variance, corresponding to a Mott state with vanishing compressibility $\frac{\partial n_+}{\partial \mu}$. These Mott lobes are surrounded by a superfluid sea where the compressibility is finite. For weak values of J/U , the lower Mott plateaus are still well visible, whereas the higher plateaus are almost all smoothed out. This is exemplified in Fig. 2c for $J'/U = 0.6$ and $J/U = 0.015$ where the variance of the first two Mott phases are still small. Between the plateaus, the variance displays maxima revealing the superfluid phases. For $\mu \gtrsim U$, n_+ varies smoothly and the system is superfluid. For larger value of J/U , the half-integer Mott lobes almost entirely disappear except at very low values of J'/U , see Fig. 2b obtained at $J/U = 0.04$. This is exemplified by Fig. 2d at $J'/U = 0.6$, where both n_+ and δn_+ vary smoothly as μ is increased. The evolution of the probability amplitudes $g_{p,q}^\ell$ when J increases and J' is fixed, is similar to the usual MI-SF scenario in the Gutzwiller's ansatz. When J'/U is large, the Mott state is approximated by the Fock

state $|p_0, +; 0, -\rangle_\ell$ and $g_{p,q}^\ell = \delta_{pp_0} \delta_{q0}$. At the transition, the distribution $g_{p,q}^\ell$ starts broadening, but only in the *symmetric* direction $q = 0$ and the physics takes entirely place in the symmetric subspace. For instance, in the limit $J' \gg J \gg U$, the superfluid phase for a density ρ is described by a coherent state in the symmetric space and no bosons in the anti-symmetric space, $|\sqrt{\rho}\rangle_+ \otimes |0\rangle_-$. At intermediate values of J' , the Mott state is slightly contaminated by anti-symmetric contributions. However, we have checked that the MI-SF transition scenario remains the same: $g_{p,q}^\ell$ still spreads along the symmetric direction and keep a structure similar to (4).

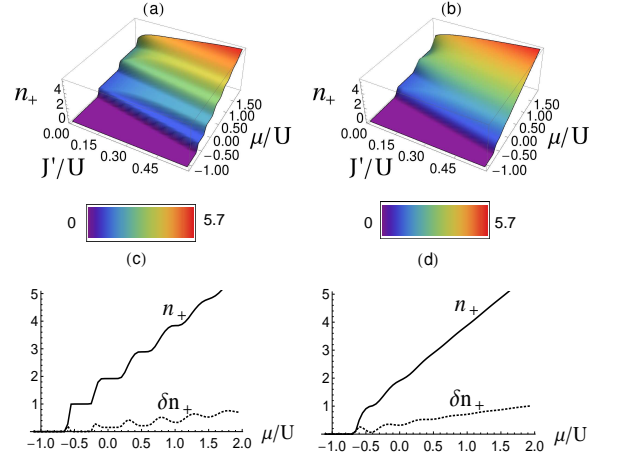


Figure 2. (color online). Left column: phase diagram of Hubbard Hamiltonian (1) for $J/U = 0.015$. Right column: same as the left column but for $J/U = 0.04$. (a), (b): occupation number n_+ as a function of J'/U and μ/U and the color code. (c), (d) n_+ and δn_+ as a function of μ/U for $J'/U = 0.6$. For $J = 0.015$, the first three Mott plateaus are clearly visible whereas they are smoothed out for $J = 0.04$.

Critical hopping amplitude. We obtain the MI-SF critical hopping rate $J_c(J'/U, \mu/U)$ by monitoring the tip of the two first Mott lobes, see Fig. 3. Within the usual Bose-Hubbard model, one predicts $U/J_{cz}^{(\rho)} = z(2\rho + 1 + 2\sqrt{\rho(\rho + 1)})$ where z is the coordination number of the lattice [17, 18] and where the integer ρ is the average density. For small J'/U , the system is made of almost independent 1D chains ($z = 2$) and the physics is driven by on-site Fock states. The main Mott lobe is at $\rho = n = 1$ (equivalently $n_+ = 2$). For imbalanced hopping parameters, one gets $(2J + J') = U/5.8$ and thus $J_c = J_{c2}^{(1)} - J'/2$. This prediction correctly reproduces our numerical results for small values of J'/U . However, in the large J'/J limit, the physics takes place in the symmetric subspace. It is easy to see from Eq. (1) that each state $|+\rangle$ is connected to $z = 4$ nearest-neighbors with an effective hopping parameter $J/2$ giving rise to a non-interacting band with finite width $4J$ independent

of J' . Furthermore, with the help of Eqs (1) and (4), a second-order perturbation shows that, in the large- J' limit, $J_c = J_{c4}^{(1)} (1 - \frac{1}{8} \frac{U}{J'})$, in good agreement with our numerical data for $\rho = n_+ = 1$ (equivalently $n = 0.5$). Remarkably, for large J'/U , the Mott lobe at $n = 1$ ($n_+ = 2$) saturates, as it should, at the value $J_{c4}^{(2)}$ ($z = 4$, $\rho = n_+ = 2$). Finally, even though the present ansatz favors one link over the two others, it is quite remarkable that our numerical results for the Mott lobe at $\rho = n = 1$ ($n_+ = 2$) cross the critical value $J_{c3}^{(1)}$, corresponding to the balanced honeycomb lattice, roughly when $J_c = J'$. From that point of view, the system undergoes a cross-over from a quasi-1D situation with two neighbors (weakly-coupled chains) to a 2D situation with four neighbors, the balanced honeycomb lattice with 3 neighbors being the intermediate situation. A thorough study of this crossover is beyond the scope of this Letter and will be published elsewhere.

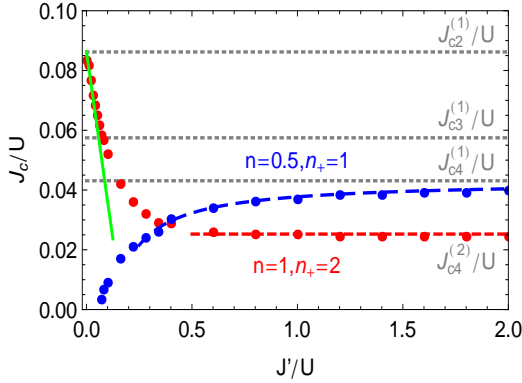


Figure 3. (color online) Critical value J_c for the MI-SF transition as a function of J' (in units of U). The red (resp. blue) dots are the numerical values obtained with the extended Gutzwiller's ansatz for the $n = 1$ (resp. $n = 0.5$) Mott lobe. Continuous and long-dashed lines are analytical predictions. The horizontal black dashed lines correspond to the critical values $J_{cz}^{(1)}$, $z = 1, 2, 3$. See text for details.

Experimental signatures. A clear signature of the MI-SF transition can be observed in the velocity distribution of the atoms when the optical lattice is rapidly switched off [12, 24]. The velocity distribution is then simply the momentum distribution in the ground state, $n_{\mathbf{k}} \propto \sum_{i,j} \langle GS | c_i^\dagger c_j | GS \rangle \exp[i\mathbf{k} \cdot (\mathbf{R}_j - \mathbf{R}_i)]$, where \mathbf{R}_i is the position of the site i . In the usual Gutzwiller's ansatz, there is no correlation between different sites and only terms like $\langle c_i^\dagger c_i \rangle$ or $\langle c_i^\dagger \rangle \langle c_j \rangle \exp(i\mathbf{k} \cdot (\mathbf{R}_j - \mathbf{R}_i))$ contribute to the signal. With the extended ansatz, we obtain additional contributions from terms like $\langle a_\ell^\dagger b_\ell \rangle \exp(i\mathbf{k} \cdot \mathbf{c}_1)$. These nearest-neighbor correlations result in an additional modulation of the velocity distribution, a smoking-gun of a Mott phase build on a symmetric state. For the Fock state $|p, +; 0, -\rangle$, one obtains $n_{MI}(\mathbf{k}) = p(1 + \cos(\mathbf{k} \cdot \mathbf{c}_1))$. A more accurate description using

Eq. (4) would show that the modulation amplitude is a direct measurement of the purity of the ground-state. For the superfluid state, a product of on-site coherent states, one finds $n_{SF}(\mathbf{k}) = \rho_0 \sum_{ij} e^{i\mathbf{k} \cdot (\mathbf{R}_j - \mathbf{R}_i)}$ (assuming a uniform density ρ_0), which depicts peaks at the reciprocal lattice vectors modulated by the square of the structure factor of the lattice. The additional on-link correlations will thus show up as an additional modulation on the top of this ideal distribution. The latter properties are confirmed by our numerical calculations, shown in Fig. 4, where, choosing \mathbf{c}_1 along Ox , both the superfluid (left plot) or the Mott (right plot) phases display a periodic modulation along k_x (stripes) with period 2π . Note that, beside the preceding modulation, the effect of the structure factor in the superfluid phase is clearly visible in the different peak heights.

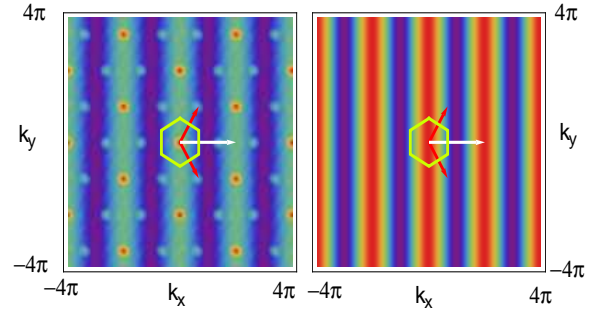


Figure 4. (color online) Velocity distribution for $J/U = 0.015$, $J'/U = 0.6$. Left frame: superfluid phase ($\mu/U = -0.14$). Right frame: Mott-insulator phase ($\mu/U = -0.5$). The hexagon is the first Brillouin zone with its reciprocal lattice vectors (red arrows). Vector \mathbf{c}_1 is chosen along Ox . The stripes along k_x (with a period 2π shown by the white arrow) are a signature of the quantum correlations between the A and B sites along \mathbf{c}_1 -links. See text for details.

In conclusion, using an extended Gutzwiller's ansatz, we have described the properties of the MI-SF transition of ultracold bosons in a honeycomb lattice. We have found Mott phases at *half-integer* fillings, arising directly from the interplay between quantum correlations and the topology of the honeycomb lattice. Future work will address the excitations of the system as they can lead to additional experimental signatures [25]. Finally, it would be interesting to study the impact of an external (non-Abelian) gauge field on the properties of the ground state [26–28]. The Centre for Quantum Technologies is a Research Centre of Excellence funded by the Ministry of Education and National Research Foundation of Singapore. This work has been supported by the CNRS-CQT LIA FSQ. ChM is a Fellow of the Institute of Advanced Studies (NTU).

[1] K.S. Novoselov, *et al.*, Science **306**, 666 (2004).

- [2] A.H. Castro Neto, *et al.*, Rev. Mod. Phys. **81**, 109 (2009).
- [3] Z. Y. Meng, T. C. Lang, S. Wessel, F. F. Assaad, and A. Muramatsu, Nature **464**, 847 (2010).
- [4] S.-L. Zhu, B. Wang, and L.-M. Duan, Phys. Rev. Lett. **98**, 260402 (2007).
- [5] K.L. Lee, B. Grémaud, R. Han, B.-G. Englert, and C. Miniatura, Phys. Rev. A **80**, 043411 (2009).
- [6] P. Soltan-Panahi, *et al.*, Nature Physics **7**, 434 (2011).
- [7] P. Soltan-Panahi, *et al.*, Nature Physics **8**, 71 (2012).
- [8] L. Tarruell, D. Greif, T. Uehlinger, G. Jotzu and T. Esslinger, Nature **483**, 302305 (2012).
- [9] D. Greif, T. Uehlinger, G. Jotzu, L. Tarruell, T. Esslinger, arXiv:1212.2634 (2012).
- [10] S. Sachdev *Quantum Phase Transitions* (Cambridge Univ. Press, Cambridge 2001).
- [11] , D. Jaksch, *et al.* Phys. Rev. Lett. **81**, 3108 (1998).
- [12] M. Greiner, O. Mandel, T. Esslinger, T. W. Hänsch and I. Bloch, Nature **415**, 3944 (2002).
- [13] M. Rigol, G. G. Bartrouni, V. G. Rousseau and R. T. Scalettar, Phys. Rev. A **79**, 053605 (2009).
- [14] I. B. Spielman, W.D. Phillips and J. V. Porto, Phys. Rev. Lett. **98**, 080404 (2007).
- [15] I. B. Spielman, W.D. Phillips and J. V. Porto, Phys. Rev. Lett. **100**, 120402 (2008).
- [16] I. Kimchi, S. A. Parameswaran, A. M. Turner and A. Vishwanath, arXiv:1207.0498 [cond-mat.str-el].
- [17] Zwerger W 2003 J. Opt. B: Quantum Semiclass. Opt. **5** S9.
- [18] A. Georges, in *Ultra-cold Fermi Gases*, Proceedings of the International School of Physics Enrico Fermi, Varenna, 20-30 June 2006, Course CLXIV, edited by M. Inguscio, W. Ketterle and C. Salomon, IOS Press (Amsterdam), p. XXX (2007).
- [19] C. Trefzger, C. Menotti, B. Capogrosso-Sansone and M. Lewenstein, J. Phys. B: At. Mol. Opt. Phys. **44**, 193001 (2011).
- [20] M. P. A. Fisher, P. B. Weichman, G. Grinstein and D. S. Fisher, Phys. Rev. B **40**, 546 (1989).
- [21] W. Ketterle, D. S. Durfee, and D. Stamper-Kurn, in *Bose-Einstein Condensation in Atomic Gases*, Proceedings of the International School of Physics Enrico Fermi, Varenna, 7-17 July 1998, Course CXL, edited by M. Inguscio, S. Stringari and C. Wieman, IOS Press (Amsterdam), p. 67 (1999).
- [22] G. Montambaux, F. Piéchon, J.-N. Fuchs, and M.O. Goerbig, Phys. Rev. B **80**, 153412 (2009).
- [23] M. Lewenstein *et al.*, Adv. in Physics **56**, 243 (2007).
- [24] I. Bloch, J. Dalibard and W. Zwerger, Rev. Mod. Phys. **80**, 885 (2008).
- [25] T. Stöferle, H. Moritz, C. Schori, M. Köhl and T. Esslinger, Phys. Rev. Lett. **92**, 130403 (2004).
- [26] A. Górecka, B. Grémaud and C. Miniatura, Phys. Rev. A **84**, 023604 (2011).
- [27] J. Dalibard, F. Gerbier, G. Juzeliūnas, P. Öhberg, Rev. Mod. Phys. **83**, 1523 (2011).
- [28] A. Bermudez *et al.*, New J. Phys. **12**, 033041 (2010).